

## Section 4

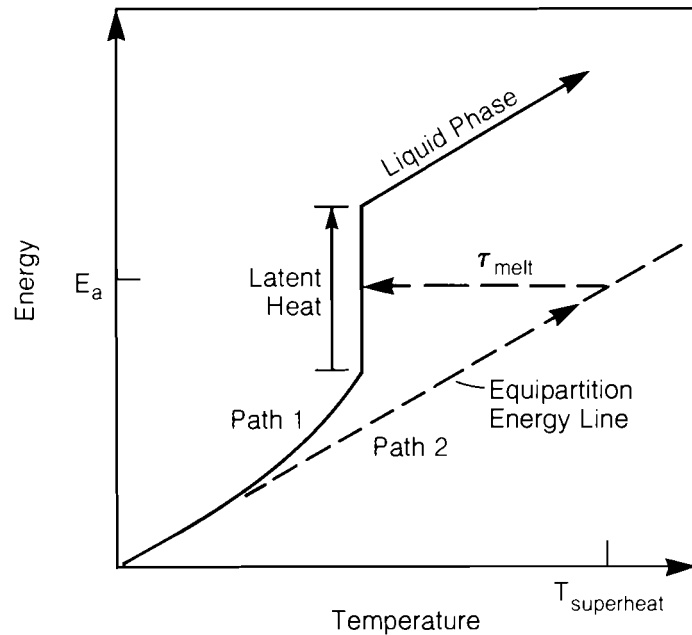
# PICOSECOND RESEARCH

### 4.A Genesis of Melting

The fundamental process responsible for initiating the melting of condensed matter has remained a mysterious and as yet unsolved problem. The longstanding interest in this most basic of phase transitions has nevertheless resulted in a great number of theoretical interpretations. The key question still to be answered is: What happens on the atomic scale when a crystal melts?

The only theory that deals with an actual microscopic mechanism capable of initiating a melt is the Defect Theory of Melting.<sup>1</sup> This model describes the formation of the liquid phase from the generation of defects: vacancies,<sup>2</sup> interstitials,<sup>3</sup> or dislocations.<sup>4</sup> The theory happens to be also consistent with the Lindemann Criterion, which is the only generally valid observation that defines at what stage melting occurs. However, as with all theories on melting, there has not been any experimental verification because of the difficulty in making a microscopic observation on a time scale appropriate to the ongoing process.

In the past ten years the short-pulse laser has evolved as an ideal tool for studying phase transitions. In addition to supplying energy densities large enough to create a melt in a time much shorter than the transition time, the optical pulse can also be used to probe the melting substance. An important consequence of this feature is that we can now drive a solid to a super-heated temperature faster than the system can respond. Figure 24.28 shows a conventional phase



E3882

Fig. 24.28  
 Caloric diagram of the solid and liquid phases for a simple metal. Path 1 is followed when the energy is deposited on a time scale slower than the defect formation time. Path 2 is followed when the energy is deposited instantaneously.

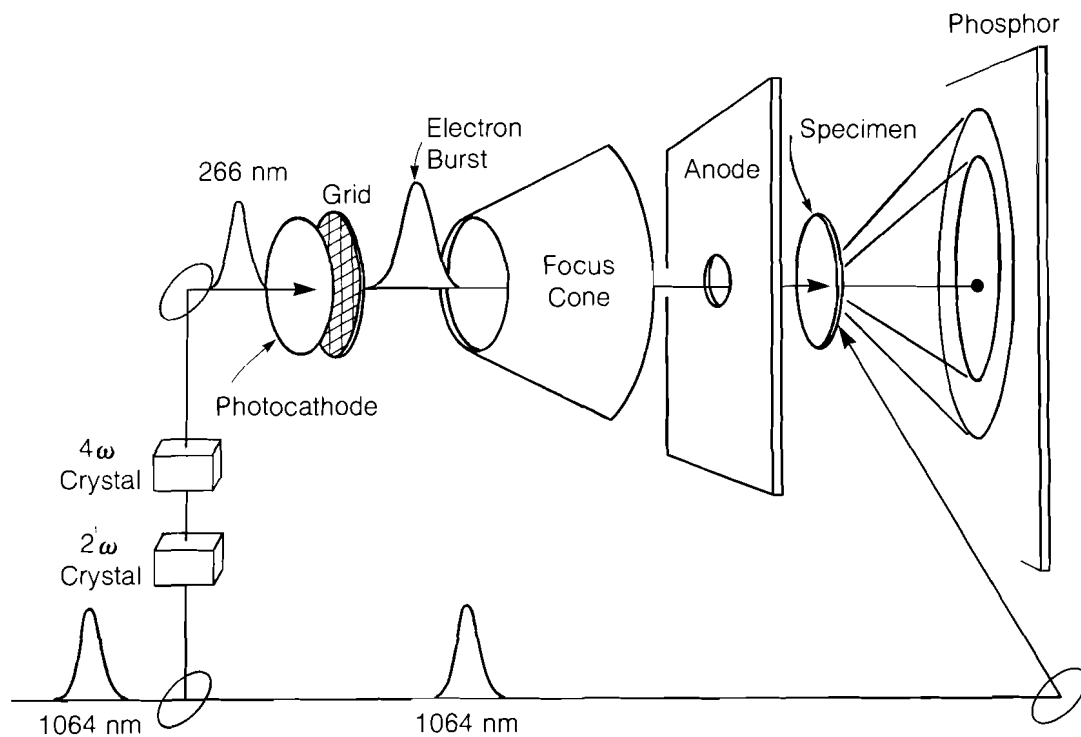
diagram where Path 1 is followed under normal equilibrium conditions. If a quantity of energy  $E_a$  is rapidly deposited into the system, the path taken is along the equipartition energy line (Path 2). Depending on the peak power of the laser pulse and the system in question, the range over which superheating occurs is several thousand degrees. The time  $\tau_{melt}$  is then the actual material-dependent melting time. The departure of Path 1 from the equipartition line is indicative of defect formation. With the short-pulse laser and a suitable probe, the rate of defect formation even below the melt threshold can be time resolved.

Several probe techniques have now been developed to time resolve phase transformations in semiconductors during laser annealing. However, most of these probes (e.g., electrical conductivity,<sup>5,6</sup> optical reflection,<sup>7,8</sup> optical transmission,<sup>9</sup> Raman scattering,<sup>10</sup> and time-of-flight mass spectrometry<sup>11</sup>) supply no direct information about the atomic structure or the temperature of the material. Probing the structure can reveal when and to what degree a system melts as it is defined by degradation in the long-range order of the lattice. True structural probes based on x-ray<sup>12</sup> and low-energy electron diffraction,<sup>13</sup> and EXAFS<sup>14</sup> with nanosecond time resolution, have been developed offering fresh insight into both the bulk and surface dynamics of material structure. Also, a subpicosecond probe based on structurally dependent second-harmonic generation<sup>15</sup> has been demonstrated. But at present, only the technique of picosecond electron diffraction<sup>16</sup> can produce an unambiguous picture of the atomic structure on the picosecond time scale.

In this article we describe an experiment utilizing this instrument to time resolve the laser-induced phase transition in aluminum. The results are then interpreted in the context of the defect theory of melting.

### Experiment and Results

The technique takes advantage of the strong scattering efficiency of 25-keV electrons in transmission mode to produce and record a diffraction pattern with as few as  $10^4$  electrons in a pulse of 20-ps duration. The burst of electrons is generated from a modified streak camera that, via the photoelectric effect, converts an optical pulse to an electron pulse of equal duration.<sup>17</sup> Also of importance is that the electron pulse can be synchronized with picosecond resolution to the laser pulse.<sup>18</sup> The experimental arrangement is illustrated in Fig. 24.29. A single pulse from an active-passive mode-locked Nd<sup>3+</sup>:YAG laser is spatially filtered and amplified to yield energies up to 10 mJ. The streak tube (deflection plates removed), specimen, and phosphor screen are placed in vacuum at  $10^{-6}$ -mm Hg. The electron tube is comprised of the photocathode, extraction grid, focusing cone, and



E2247

Fig. 24.29

Schematic of picosecond electron diffraction apparatus. A streak camera tube (deflection plates removed) is used to produce the electron pulse. The 25-keV electron pulse passes through the Al specimen and produces a diffraction pattern of the structure with a 20-ps exposure.

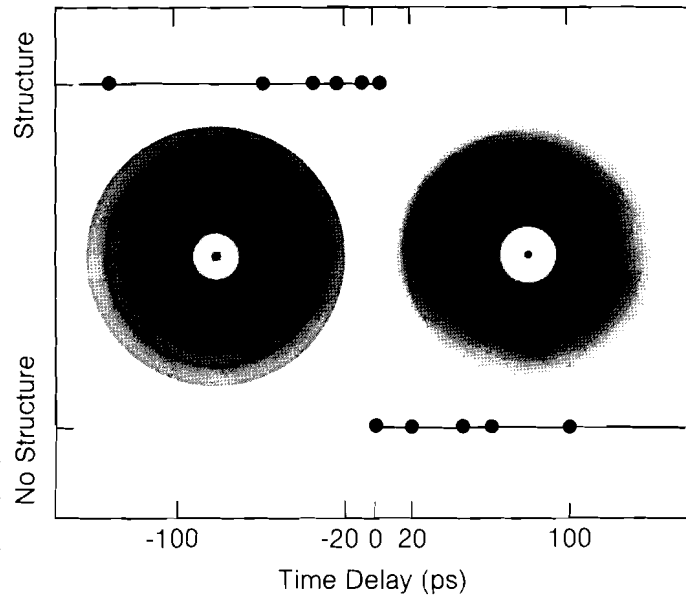
anode. A gold photocathode is used to permit the vacuum chamber to be opened to air. The photocathode is held at the maximum voltage ( $-25$  kV) so that space charge, which can cause significant temporal broadening, is minimized. The portion of the laser irradiating the photocathode is first up-converted to the fourth harmonic of the fundamental wavelength in order to produce the electrons efficiently. The duration of the UV pulse, and thus the electron pulse, is  $\sim 20$  ps. Once the electron pulse is generated it accelerates through the tube past the anode and then remains at a constant velocity. The specimen is located in this drift region. The electrons pass through the specimen with a beam diameter of  $500 \mu\text{m}$  and come to a  $200\text{-}\mu\text{m}$  focus at their diffracted positions on the phosphor screen. A gated-microchannel-plate image intensifier in contact with the phosphor screen amplifies the electron signal  $\sim 10^4$  times.

A metal was chosen over a semiconductor as the specimen because of the ease with which metals can be fabricated in ultra-thin polycrystalline films. The specimens were fabricated by first depositing Al onto formvar substrates and then vapor-dissolving away the formvar. Freestanding films  $250 \pm 20 \text{ \AA}$  in thickness were required so that the electrons sustain, on the average, one elastic collision while passing through the specimen. This thickness of Al corresponds to twice the  $1/e$  penetration depth at  $1060 \text{ nm}$ . It is worth noting that the penetration depth for a metal does not vary significantly from solid to liquid, as is the case with a semiconductor where a change in absorption of one to two orders of magnitude is possible. Since the diffusion length  $(D\tau)^{1/2}$ —where  $D$  is the thermal diffusivity coefficient ( $0.86 \text{ cm}^2/\text{s}$ ) and  $\tau$  is time—is limited to  $250 \text{ \AA}$ , the temperature in the Al is uniformly established in less than  $10$  ps. The absorption of the laser by aluminum is  $13 \pm 1\%$ .

The diameter of the laser stimulus is  $\sim 4 \text{ mm}$  ( $1/e^2$ ) and is centered over the  $2\text{-mm}$  specimen. A  $1\text{-mm}$  pinhole, positioned in place of the specimen, facilitates accurate alignment of the laser beam profile to the electron beam. Using a  $1\text{-mm}$  pinhole assures accurate measurement of the fluence within the probed region. Synchronization between the electron pulse and the laser stimulus is then accomplished by means of a laser-activated deflection plate assembly.<sup>19</sup>

The experimental procedure is then to stimulate the aluminum sample with the laser while monitoring the lattice structure at a given delay. The films are used only once, even though for low fluence levels ( $\leq 8 \text{ mJ/cm}^2$ ) the films could survive repeated shots. Figure 24.30 shows the laser-induced time-resolved phase transformation of aluminum at a constant fluence of  $\sim 13 \text{ mJ/cm}^2$ . The abrupt disappearance of rings in the diffraction pattern occurs with a delay of  $20$  ps. As is evident, the breakdown of lattice order can be induced in a time shorter than the resolution of our probe. However, the fluence required for this rapid transition exceeds  $F_{\text{melt}}$ , the calculated fluence required to completely melt the Al specimen under equilibrium conditions ( $\sim 5 \text{ mJ/cm}^2$ ). At a constant fluence of  $11 \text{ mJ/cm}^2$  the phase transition was again observed, but only after a probe delay of  $60$  ps. Figure 24.31 shows the melt metamorphosis of Al, where the points represent the

Fig. 24.30  
Time-resolved laser-induced phase transition in aluminum. The pattern on the left is the diffraction pattern for Al and represents the points along the top line—where the electron pulse arrives before the laser stimulus. The pattern on the right shows the loss of structure in the Al 20 ps (or more) after applying the laser stimulus at a fluence of 13 mJ/cm<sup>2</sup>. The fine line background structure occurring in both pictures is an artifact of the circular averaging technique.



E2873

delay time before the complete phase transition is observed for various fluence levels. We see that the elapsed time increases exponentially with decreased fluence, and at 7 mJ/cm<sup>2</sup> the delay is ~ 1 ns. Because the fluence level that is applied is always in excess of  $F_{\text{melt}}$ , the observed delay time suggests that the Al is first driven to a superheated solid state before melting. It must be pointed out that as the fluence was decreased the abruptness with which the rings disappeared became less dramatic. Consequently, determination of the precise delay increases in difficulty with decreasing fluence. The temperature scale represents the temperature of the superheated Al, assuming a linear increase in the specific heat with temperature. We see that temperatures in excess of 2000°K are expected, with fluence levels near 13 mJ/cm<sup>2</sup>. The region beneath the curve represents the conditions under which the Al can be observed in a superheated solid state.

#### Interpretation

Let us assume that the disorder is induced by the generation of either vacancies or interstitials. The jumping frequency is then given by

$$v_j = \nu \exp \left( - \frac{E}{kT} \right),$$

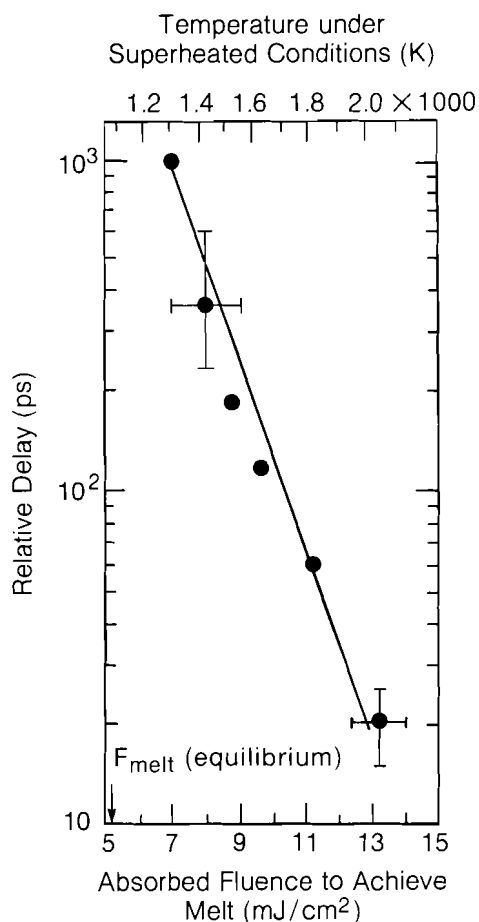
where  $\nu$  is the atomic vibrational frequency and  $E$  is the activation energy (1 eV for Schottky type, ~ 4 eV for Frenkel type, and 1 eV for self-diffusion).

If we further assume that a fixed number of vacancies is required to initiate the melt, we can then find the activation energy  $E$  from the slope

of the curve in Fig. 24.31

$$E = K \frac{\partial(\ln \tau_{ob})}{\partial(1/T)} = 1 \pm 0.2 \text{ eV,}$$

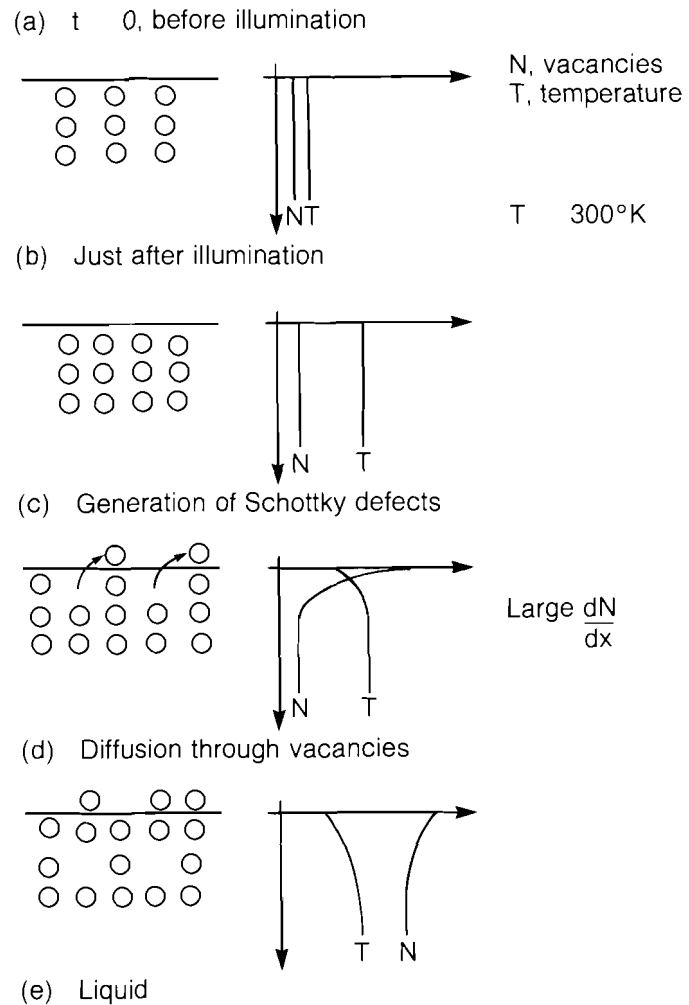
where T is temperature and  $\tau_{ob}$  is the corresponding decay time for the melting process to be completed.



E2864

Fig. 24.31  
Laser-induced melt metamorphosis for aluminum. The points mark the elapsed time for the diffraction rings to completely disappear. The vertical error bar represents the degree of uncertainty in defining the moment of complete melt. The region beneath the curve represents the conditions under which the Al is left in a superheated solid state.

The activation energy agrees surprisingly well with the required energy for Schottky defect formation, which suggests that the melt actually begins at the outer surfaces of the individual crystallites and propagates inward through self-diffusion. Figure 24.32 depicts a possible ultrafast scenario that is founded on the defect theory of melting. Just after illumination, the lattice is uniformly hot; surface defects then begin to form, cooling the lattice. A temperature gradient, corresponding to the defect gradient, is thus established. The two gradients persist until the crystal is saturated with defects and is said to be homogeneously melted.



E3510

Fig. 24.32  
Scenario for ultrafast melting based on the  
Defect Theory of Melting.

In conclusion, we have demonstrated that the picosecond electron-diffraction technique can be used to provide time resolution of the laser-induced melt evolution in aluminum. We found it possible to melt the aluminum completely in a time shorter than 20 ps if sufficient laser fluence is applied ( $\geq 2.6 \times F_{\text{melt}}$ ). The time required to melt the aluminum increases exponentially with decreasing fluence; at  $1.4 \times F_{\text{melt}}$ , the phase transition time increased to  $\sim 1$  ns. During this time, the two phases coexist as a heterogeneous melt while the superheated solid is being continuously transformed into liquid. We have interpreted the results in terms of the defect theory of melting and found that the activation energy measured agrees with that of Schottky defect formation.

## ACKNOWLEDGMENT

This work was supported by the following sponsors of the Laser Fusion Feasibility Project at the Laboratory for Laser Energetics—Empire State Electric Energy Research Corporation, General Electric Company, New York State Energy Research and Development Authority, Northeast Utilities Service Company, Ontario Hydro, Southern California Edison Company, The Standard Oil Company, and University of Rochester. Such support does not imply endorsement of the content by any of the above parties.

The authors would like to acknowledge the support of Jerry Drumheller, who assisted in the fabrication of the aluminum films, as well as to thank Hsiu-Cheng Chen for her help during the experiment.

## REFERENCES

1. F. C. Frank, *Proc. R. Soc. London, Ser. A* **170**, 182 (1939).
2. J. Frenkel, *Kinetic Theory of Liquids* (Dover Publications, 1955).
3. J. E. Lennard-Jones and A. F. Devonshire, *Proc. R. Soc. London, Ser. A* **169**, 317 (1939); **170**, 464 (1939).
4. D. Kuhlmann-Wildorf, *Phys. Rev. A* **140**, 1599 (1965).
5. M. Yamada *et al.*, *J. Phys. Soc. Jpn.* **49**, 1299 (1980).
6. G. J. Galvin *et al.*, *Phys. Rev. Lett.* **48**, 33 (1982).
7. D. H. Auston *et al.* *Appl. Phys. Lett.* **33**, 437 (1978).
8. C. V. Shank, R. Yen, and C. Hirlimann, *Phys. Rev. Lett.* **50**, 454 (1983).
9. J. M. Liu, H. Kurz, and N. Bloembergen, *Appl. Phys. Lett.* **41**, 643 (1982).
10. H. W. Lo and A. Compaan, *Phys. Rev. Lett.* **44**, 1604 (1980).
11. A. Pospieszczyk, M. A. Harith, and B. Stritzker, *J. Appl. Phys.* **54**, 3176 (1983).
12. B. C. Larson, C. W. White, T. S. Noggle, and D. Mills, *Phys. Rev. Lett.* **48**, 337 (1982).
13. R. S. Becker, G. S. Higashi, and J. A. Golovchenko, *Phys. Rev. Lett.* **52**, 307 (1984).
14. H. M. Epstein, R. E. Schwerzel, P. J. Mallozzi, and B. E. Campbell, *J. Am. Chem. Soc.* **105**, 1466 (1983).
15. C. V. Shank, R. Yen, and C. Hirliman, *Phys. Rev. Lett.* **51**, 900 (1983).
16. G. Mourou and S. Williamson, *Appl. Phys. Lett.* **41**, 44 (1982).
17. D. J. Bradley and W. Sibbett, *Appl. Phys. Lett.* **27**, 382 (1975).
18. G. Mourou and W. Knox, *Appl. Phys. Lett.* **36**, 623 (1980).
19. S. Williamson, G. Mourou, and S. Letzring, *High Speed Photography*, (SPIE, Bellingham, WA, 1983), Vol. 348(I), p.197.